

Project No. 09-825

Adsorptive Separation and Sequestration of Krypton, I and C14 on Diamond Nanoparticles

Fuel Cycle

Dr. Tushar K. Ghosh

University of Missouri-Columbia

Kimberly Gray, Federal POC

Bob Jubin, Technical POC

Project No. NEUP 09-825

Adsorptive Separation and Sequestration of Krypton, I and C14 on Diamond Nanoparticles.

DOE-NEUP FINAL DOE-NEUP FINAL REPORT

Project Number: 09-825

Initiative/Campaign: AFCI/Separations

Project Title:

Adsorptive Separation and Sequestration of Krypton, I and C14 on Diamond Nanoparticles.

Principal Investigator:

Tushar K. Ghosh - University of Missouri-Columbia

Co-Investigators:

Sudarshan Loyalka - University of Missouri, Columbia
Mark Prelas - University of Missouri, Columbia
Dabir S. Viswanath - University of Missouri, Columbia

Table of Contents

Abstract.....	5
1.0 Scope of the Work	6
2.0 Research Plan.....	7
3.0 Boron Doping and Irradiation of Diamond Nano-Powders.....	8
4.0 Nano-size Diamond powder	9
4.1 Micron-size Diamond powder	9
4.1.1 Modification of Surface.....	10
4.1.2 Boron Diffusion	12
4.1.3 Cleaning Process.....	13
4.1.4 Characterization of Diamond and Boron Doped Diamond Powder	13
4.1.4.1 Surface area.....	13
4.1.4.2 SEM and EDS Analysis.....	14
4.1.4.3 XPS Analysis of Diamond Powder.....	19
4.2 Irradiation Process at the University of Missouri Research Reactor (MURR).....	26
5.0 Adsorption Measurements	28
5.1 Krypton.....	28
5.2 Iodine	33
5.3 Krypton and Iodine co-adsorption	36
6.0 Carbon dioxide Adsorption.....	37
6.1 Experimental Section	37
6.1.1 Materials	37
6.1.1.1 Adsorbents	Error! Bookmark not defined.
6.1.1.2 Adsorbates.....	Error! Bookmark not defined.
6.1.2 Static Adsorption Apparatus	37
7.0 Process Optimization	43
7.1 Material Balance in a Packed Bed Adsorbed.....	43

8.0 References:..... 46

Abstract

The objective of this research proposal was to address the separation and sequestration of Kr and I from each other using nano-sized diamond particles and retaining these in diamond until they decay to the background level or can be used as a byproduct. Following removal of Kr and I, an adsorbent will be used to adsorb and store CO₂ from the CO₂ rich stream.

A Field Enhanced Diffusion with Optical Activation (FEDOA-a large scale process that takes advantage of thermal, electrical, and optical activation to enhance the diffusion of an element into diamond structure) was used to load Kr and I on micron or nano sized particles having a larger relative surface area. The diamond particles can be further increased by doping it with boron followed by irradiation in a neutron flux. Previous studies showed that the hydrogen storage capacity could be increased significantly by using boron-doped irradiated diamond particles.

Diamond powders were irradiated for a longer time by placing them in a quartz tube. The surface area was measured using a Quantachrome Autosorb system. No significant increase in the surface area was observed. Total surface area was about 1.7 m²/g. This suggests the existence of very minimal pores. Interestingly it showed hysteresis upon desorption. A reason for this may be strong interaction between the surface and the nitrogen molecules.

Adsorption runs at higher temperatures did not show any adsorption of krypton on diamond. Use of a GC with HID detector to determine the adsorption capacity from the breakthrough curves was attempted, but experimental difficulties were encountered.

1.0 Scope of the Work

The objective of this research proposal was to address the separation and sequestration of Kr and I from each other using nano-sized diamond particles and retaining it in diamond until they decay to the background level or are used as a byproduct. Due to the size difference among these atoms/molecules, it was expected that, by optimizing the process variables, they could be separated from each other in a stage-wise separation and simultaneously stored in diamond. Following removal of Kr and I an adsorbent could be used to adsorb and store CO₂ from the CO₂ rich stream. Measurements of adsorption of Kr and I on processed diamond powders, as well as CO₂ adsorption on suitable adsorbents, were to be conducted. Also, system design for a packed bed was to be explored, as guided by the data.

2.0 Research Plan

To accomplish the objectives of this project, we planned to focus on the following tasks:

1. Boron doping and irradiation of diamond nanopowders.
2. Study pure component adsorption capacity of Kr by diamond micron and nanoparticles.
3. Study pure component adsorption capacity of I by diamond micron and nanoparticles.
4. Evaluate adsorbents for $^{14}\text{CO}_2$ capture and storage.
5. Establish time dependence of Kr and I loading on diamond (Adsorption rate).
6. Investigate adsorption capacity of Kr and I from their binary mixtures by diamond nanoparticles with and without the presence of CO_2 .
7. Optimize process parameters through Monte Carlo simulation.
8. Develop design parameters for process equipment for adsorptive separation of Kr and I.
9. Design the system for removal and long term storage of Kr, I, and CO_2 .

3.0 Boron Doping and Irradiation of Diamond Nano-Powders

Five different sizes of diamond powders were used in this work. One of these diamond powders was synthetic and in the nano-size range.

Diamond possesses several important properties including extreme hardness, high electrical resistance, chemical inertness, high thermal conductivity, high electron and hole mobilities, and optical transparency. Each carbon atom in diamond is tetrahedrally bonded to four other carbons using sp^3 -hybrid orbitals (See Figure 1). Microstructurally the atoms arrange themselves in stacked, six-member rings, with each ring in a "chair" rather than a planar configuration. In boron-doped diamond powders boron atoms substitute some of the carbon atoms.

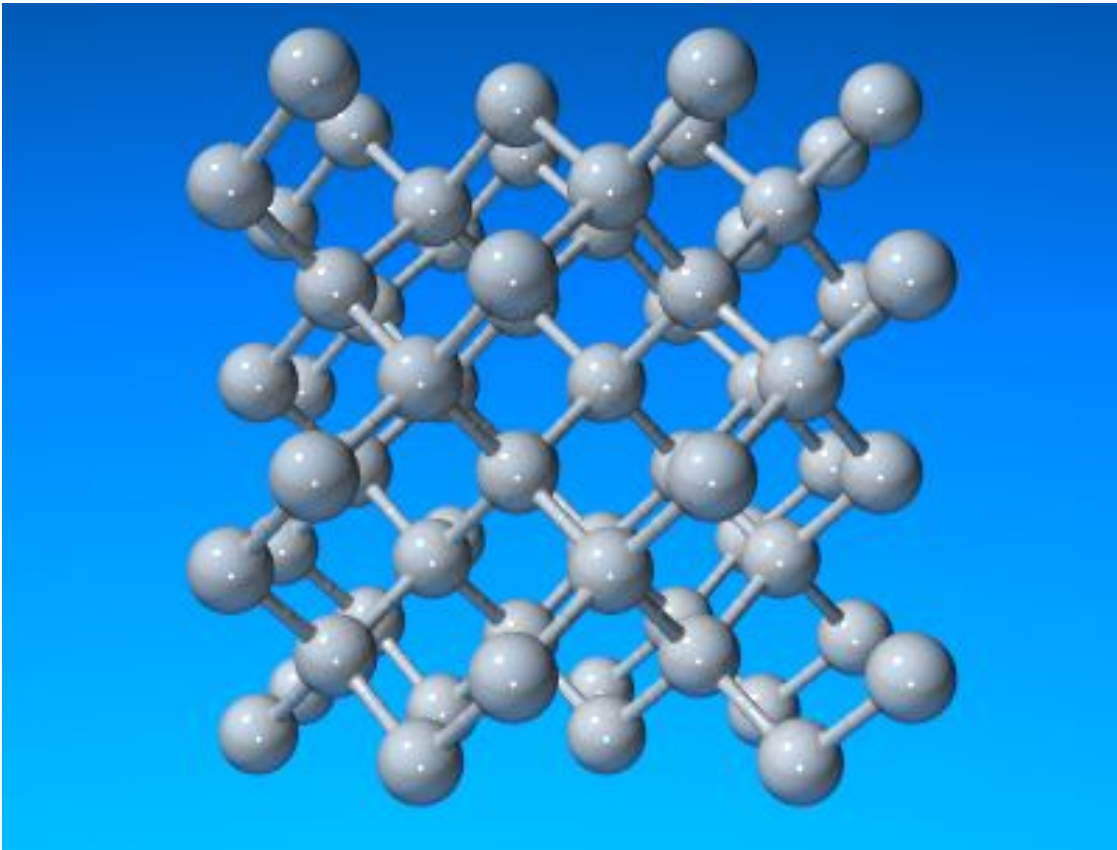


Figure 1: Structure of Diamond.

4.0 Nano-size Diamond powder

The nano-phase diamond powder (NanoDiamond, Import & Export Caspio SA) is unique in particle size and shape. The diameter of diamond crystals is in average 5 nanometers. The unique rounded shape offers superior lubricity characteristics with the hardness and wear resistance of diamond. Pure nanodiamond is produced by detonation of carbon based materials followed by chemical purification. Table 1 shows the characteristic properties of the nano-phase diamond powder.

Table 1: Characteristic properties of the nano-phase diamond powder.

Property (unit)	Values
Average monocrystal size (nm)	5
Average size of grains (nm)	20-50
Pycnometric density (g cm ⁻³)	3.2-3.2
Specific surface (m ² g ⁻¹)	~300
Initial air oxidation temperature (°C)	430
Initial vacuum graphitization temperature (°C)	1100-1200
Bulk weight (g cm ⁻³)	0.4-0.6
Constant of crystal lattice (nm)	0.3573 ± 0.0005
Beginning of air oxidation (°C)	~450
Beginning of vacuum graphitization (°C)	~1100

4.1 Micron-size Diamond powder

Type IIa transparent natural diamond crystals (Microdiamant®) with three different sizes were used in this work. The sizes were about 80, 35-45, and 5.5-8 μm. Figure 2 shows the vials that were purchased from Microdiamant.



Figure 2: Vials containing the natural micron size diamond powder from Marodiamant®.

Table 2: Properties of micron size diamond powder.

Property (unit)	Value
Density (g cm^{-3})	3.5
Bandgap Energy (eV)	5.49
Resistivity (Ohms cm)	>1012
Breakdown Voltage (V cm^{-1})	107
Electron Mobility ($\text{cm}^2 \text{V}^{-1} \text{s}^{-1}$)	2400
Hole Mobility ($\text{cm}^2 \text{V}^{-1} \text{s}^{-1}$)	2100
Saturation Velocity (km s^{-1})	220
Dielectric Constant	5.7
Energy to form e-h pair (eV)	13
Thermal Conductivity ($\text{W m}^{-1}\text{K}^{-1}$)	2000

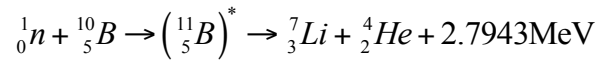
4.1.1 Modification of Surface

Diamond is a well-known promising industrial material for different applications because of its unique physical and chemical properties. Several studies have been focused on surface

modifications. They can be classified onto two main groups: modification in vapor phase, and in modification of liquid phase. In this research, modification of the surface of diamond powder was done in order to enhance its porosity. Porous carbon materials due to their tunable microtexture and surface functionality and different forms (powders) offer a wide range of possibilities for gas storage. Well-developed microporous carbon materials are needed because the higher the porosity is, the higher the adsorption capacity is.

In this work, elemental boron-powder (325-mesh) of purity 99.99 % supplied by Alfa-Aesar was used to dope diamond powders. Diamond powders were treated with boron at different temperatures. Once the boron doping was done, each sample was sent to the University of Missouri Research Reactor to be irradiated in a neutron flux.

The main reason for irradiating the sample with a neutron flux is to initiate the following reaction.



This reaction produces a high energy alpha particle that has a mean free path of approximately 4 microns. Alpha particles, which have energy of 1.474 MeV, actually damage the solid. It requires only about 45 KeV of energy to displace a carbon atom from its normal position, and each displacement will produce one micropore. Therefore, the released energy may produce several permanent defects in the solid. This creates a heavily damaged track that can be preferentially etched to produce a long narrow channel. These channels greatly enhance the interconnectivity of the micropores produced by the neutron damage. The total number of defects in the solid will depend on how long the sample is irradiated, and on the neutron flux density. The process is shown in Figure 3.

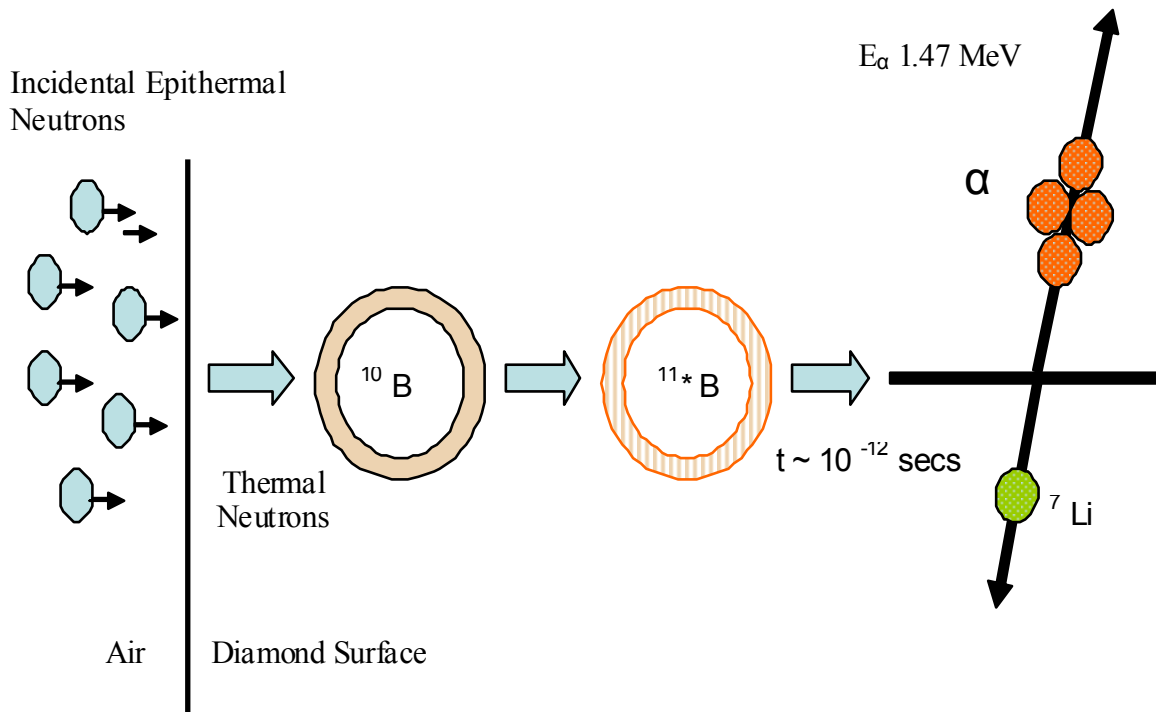


Figure 3: Schematic of Boron-10 Neutrons Reaction

4.1.2 Boron Diffusion

Three different ratios of boron to diamond were used in this study and they were 5:1, 3:1, and 2:1. Natural diamond crystals usually contain many defects including extended defects such as dislocations, voids, etc. The crystals were not characterized for the defect content before boron diffusion. In the experiment, boron and diamond powders of the ratios mentioned above were thoroughly mixed and then placed inside a ceramic boat. The boat was placed inside a ceramic tube. The ceramic tube was placed inside the tube furnace and flushed with argon or hydrogen to remove air from the ceramic tube. After 10 minutes of flushing, the heating of the furnace started while hydrogen was still flowing through the tube at a flow rate of about $10 \text{ cm}^3/\text{min}$. The experimental system is shown in Figure 4. Once the desired temperature was attained, the heating of the sample was continued for a predetermined period of time. Diamond powder was treated with boron at three different temperatures: $700 \text{ }^\circ\text{C}$, $900 \text{ }^\circ\text{C}$, and $1100 \text{ }^\circ\text{C}$. Following heating, the sample was cooled to room temperature and cleaned using various acids, which are discussed in the following section.

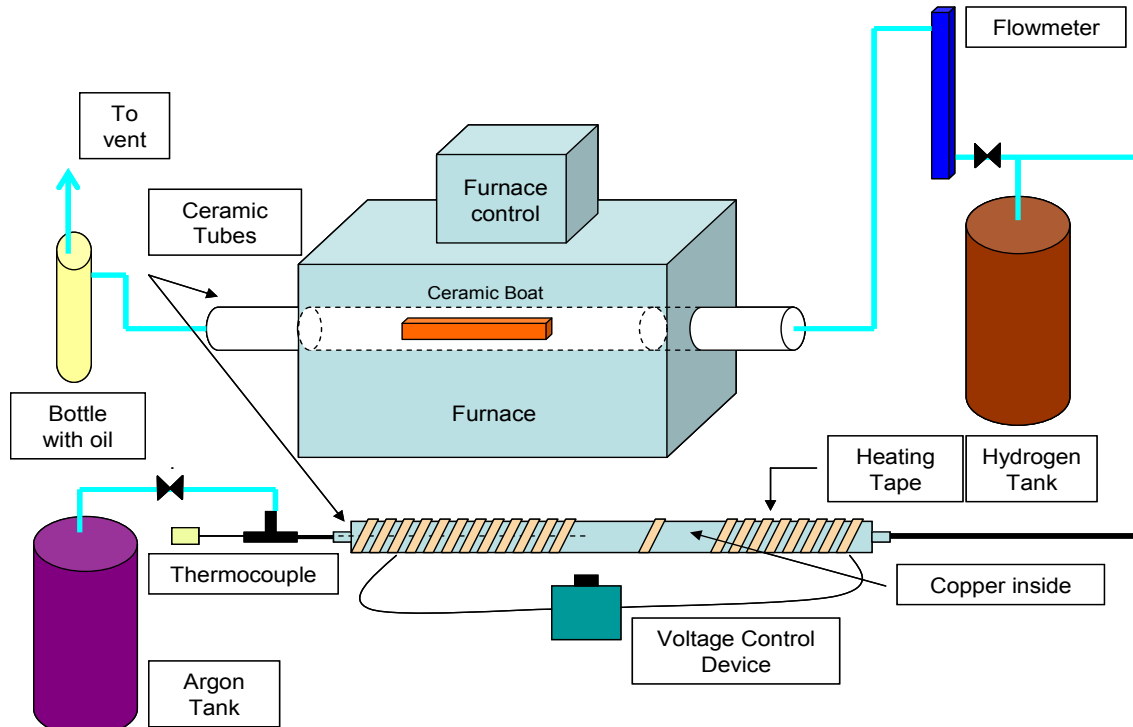


Figure 4: Dynamic setup for doping of diamond powder by boron.

4.1.3 Cleaning Process

After the diffusion process the diamond powder was cleaned in three steps. In the first step the processed powder was soaked in nitric acid (HNO_3) for three hours. In the second step the nitric acid soaked powder was boiled with chromic acid (CrO_3) for 3 hours at $200\text{ }^\circ\text{C}$ to eliminate the graphitic residues. Then a mixture of HCl , HNO_3 , and de-ionized water (ratio of 3:1:1) was used in the third step in which the powder and solution were heated for 3 hours at $200\text{ }^\circ\text{C}$ to eliminate the chromic residues. Finally, the sample was rinsed with de-ionized water several times at room temperature.

4.1.4 Characterization of Diamond and Boron Doped Diamond Powder

The untreated and boron doped diamond powders were characterized by measuring their BET surface area, and by SEM, EDS, XPS, and XRD methods.

4.1.4.1 Surface area

The BET surface area, determined at 77 K , was found to be $1.7\text{ m}^2/\text{g}$. The adsorption and desorption plot is shown in Figure 5. Interestingly, a large hysteresis loop was noted between the relative pressure range of 0.1 and 0.85. The exact reason for this kind of behavior needs to be

explored further. No significant change in the surface area was noted following irradiation in a neutron flux of the boron doped diamond powder. The boron doped diamond powder was irradiated only for 1 minute, which appears to be inadequate for significant enhancement of pore volume.

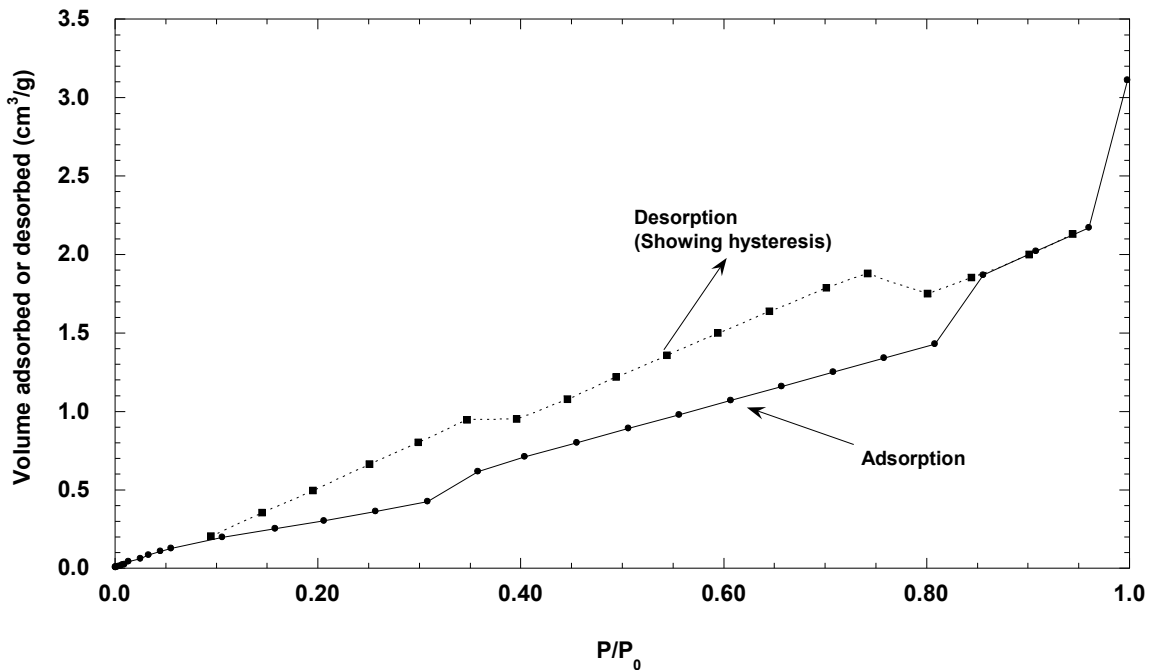


Figure 5: BET surface area of diamond powder (35-45 micron size) at 77 K.

4.1.4.2 SEM and EDS Analysis

The diamond powder was characterized by SEM and EDS to understand its surface morphology. With this technique the crystalline size and faceting in diamond structure were examined. An SEM image of untreated diamond powders is shown in Figure 6.

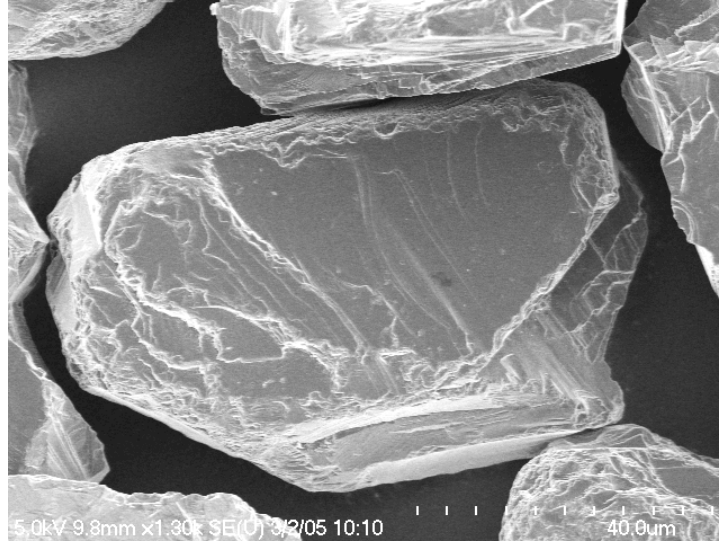


Figure 6: SEM micrograph of untreated diamond powders (5.5-8 micron)

An SEM micrograph of boron treated samples is shown in Figure 7. It shows no change in the morphology except that boron oxide particles are stuck on the surface of the crystals. The sample is shown in Figure 8 with a higher magnification where the presence of boron particles is more pronounced.

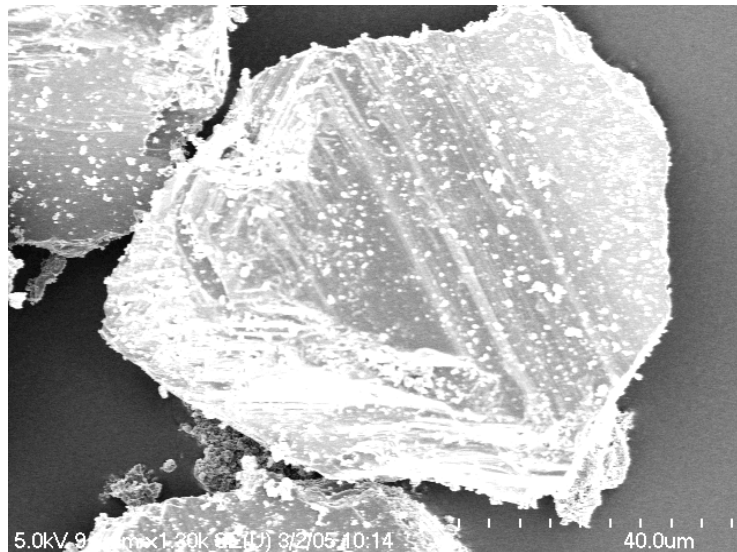


Figure 7: SEM micrograph of diamond powder (5.5-8 μm) treated with boron (white spots are boron/boron oxide stuck on the surface).

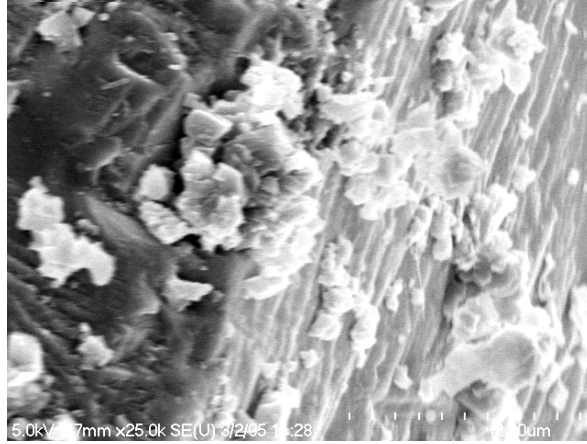


Figure 8: The SEM micrograph of boron doped diamond powder (5.5-8 μm) at higher magnification.

Energy Dispersive X-ray Spectroscopy (EDS) analysis of untreated, and boron doped samples, is shown in Figures 9 and 10 respectively. EDS analysis can provide rapid multi-element analyses. Figure 9 shows the carbon peak at around 0.28 keV for the pure diamond powder. The boron treated sample shows peaks for carbon, oxygen, and boron. The electron beam was placed directly onto one of the white spots shown in the SEM micrographs. This analysis shows that boron may be oxidized by oxygen forming boron oxide on the surface of diamond crystals. The source of oxygen may be leaked air. However, no damage of the surface was identified from the SEM micrographs. The platinum peak in the EDS spectrum is from applying a thin coating of platinum to ensure electrical conductivity for SEM/EDS.

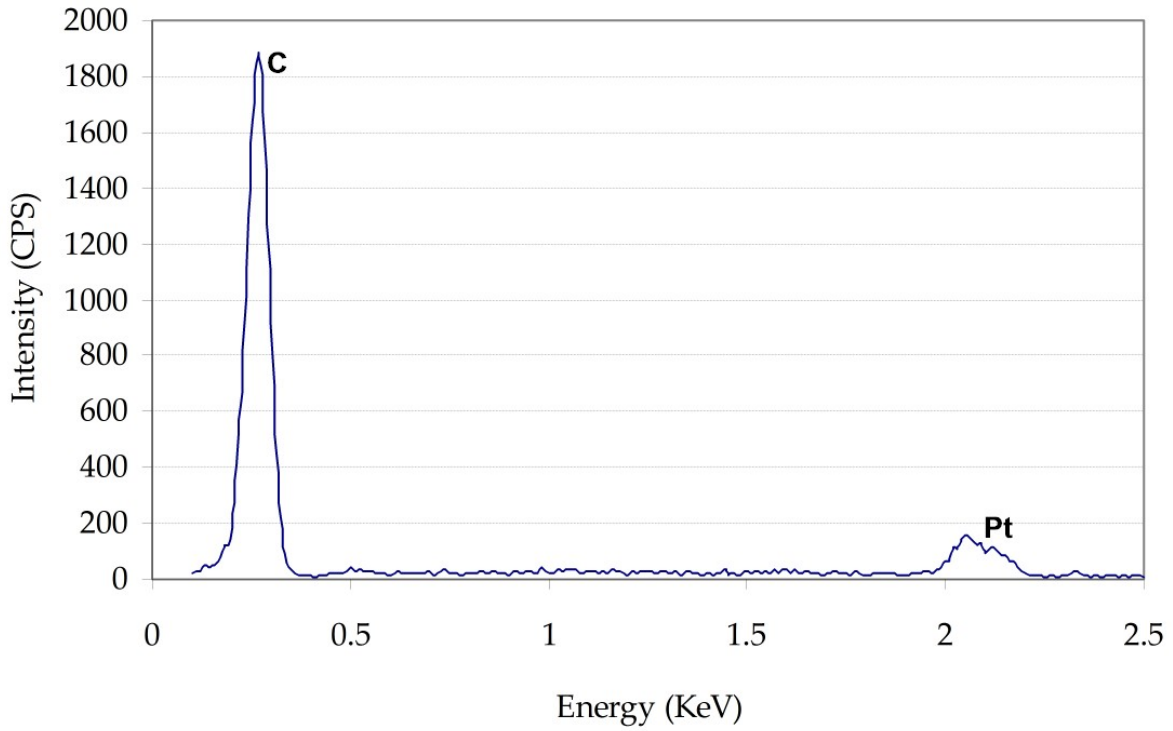


Figure 9: EDS X-ray microanalysis of untreated diamond powder (5.5-8 μm).

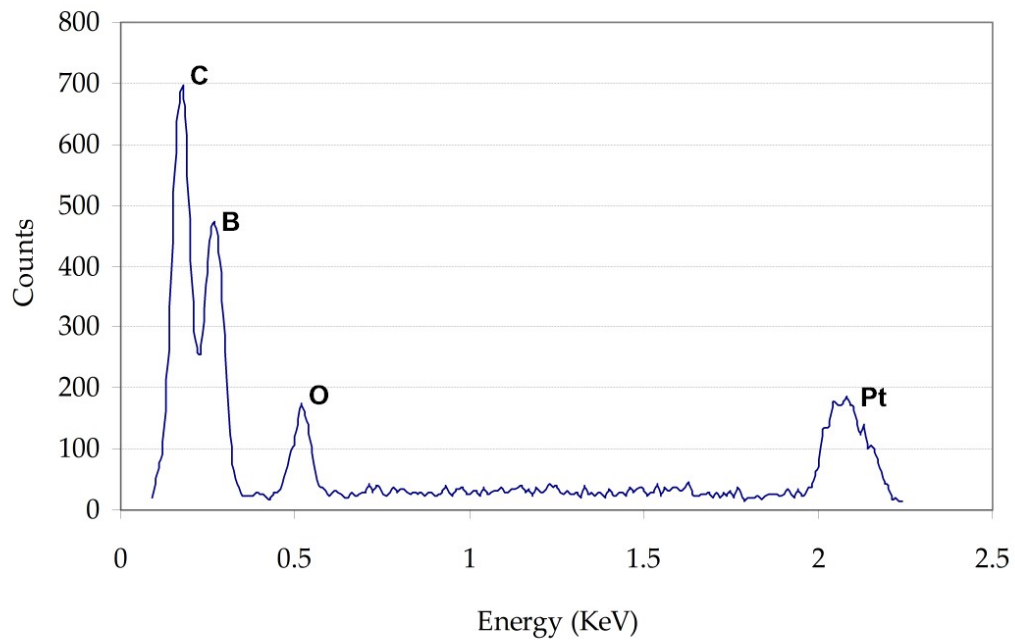


Figure 10: EDS X-ray microanalysis of diamond powder treated with boron powder and cleaned once with HNO₃.

Diamond powders in the size range of 35-45, 5.5-8, and ~0.25 microns were also treated with boron in a similar manner as described earlier. An SEM micrograph of untreated 35-45 micron diamond powder is shown in Figure 11.

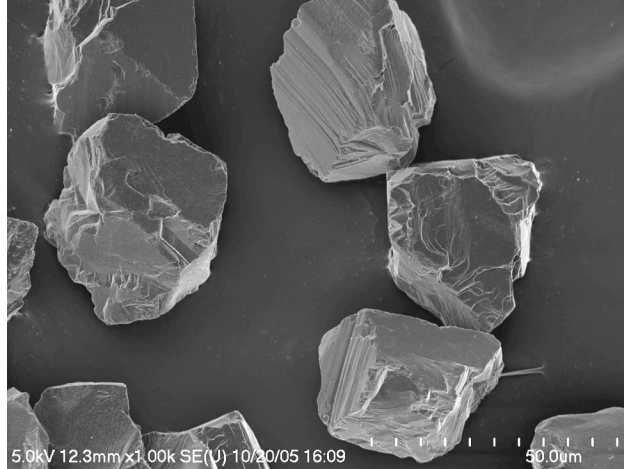


Figure 11: SEM micrographs of untreated diamond powder (35-45 μm).

As can be seen from this figure, the surface of untreated diamond powder was rather clean. An SEM of the same size diamond powder treated with boron powder for 8 hours at 1473 K is shown in Figure 12. The sample was cleaned using all three steps; however, the boron was still present on the surface.

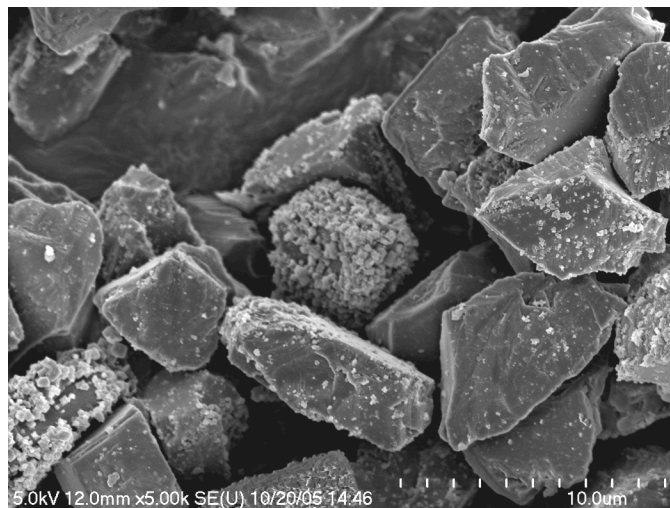


Figure 12: SEM micrograph of 35-45 micron size diamond powder treated with boron powder.

A similar result was observed with 5.5-8 micron size diamond powder that was treated with boron. An SEM micrograph of this is shown in Figure 13.

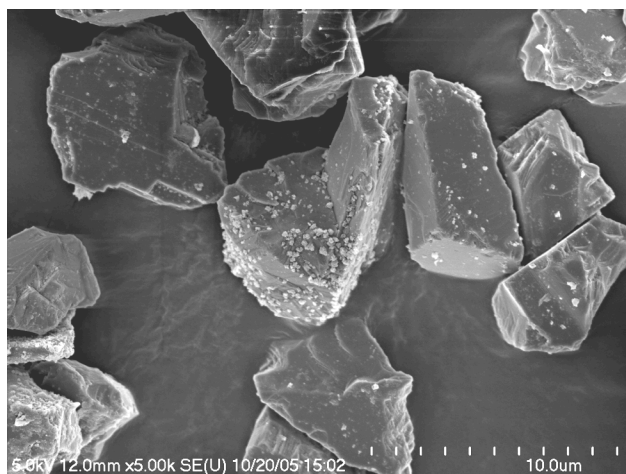


Figure 13: SEM micrograph of 5.5-8 micron size diamond powder treated with boron.

4.1.4.3 XPS Analysis of Diamond Powder

X-ray Photoelectron Spectroscopy (XPS) was used to analyze the interactions between various species on the surface of the diamond powder doped with boron. Peaks identified on pure diamond powder, 5.5-8 microns in size, are given in Table 3 along with their binding energy. As expected, only carbon and oxygen peaks were observed and the untreated sample did not show any boron on the surface.

Table 3: showed the XPS quantification report of the control sample.

Peak	Position BE (eV)	FWHM (eV)	Raw Area (CPS)	Atomic Mass	Atomic Conc. (%)	Mass Conc. (%)
O 1s	531.00	4.200	4398.4	15.999	2.49	3.29
C 1s	284.00	3.284	73312.0	12.011	97.51	96.71

Table 4 shows the binding energies of various species on the surface of the diamonds of size 35-45 microns that were treated with boron. Along with carbon and boron, other species that are identified on the surface include sodium, oxygen, nitrogen, and sulfur. The source of the sodium and the sulfur, which were present in small concentrations, could not be identified.

Table 4: XPS quantification report of sample 35-45 micron, treated with boron.

Peak	Position BE	FWHM	Raw Area	Atomic Mass	Atomic Conc.	Mass Conc.
	(eV)	(eV)	(CPS)		(%)	(%)
Na 1s	1069.50	2.048	2008.3	22.990	0.61	1.11
O 1s	530.50	2.600	20259.8	15.999	11.99	15.24
N 1s	399.00	0.965	376.9	14.007	0.32	0.36
C 1s	284.00	1.656	61141.4	12.011	85.14	81.14
B 1s	190.00	2.181	645.9	10.823	1.70	1.46
S 2p	166.50	1.259	366.0	32.065	0.23	0.59

The Carbon 1s peak is at 284.0 eV with a FWHM (Full Width at Maximum Height) of 1.656 eV. The Boron 1s peak is at 190.0 eV with a FWHM of 2.181 eV. According to Fundamental XPS Data from Pure Elements, Pure Oxides, and Chemical Compounds (XPS International Inc., 1999), carbon and boron peaks are located at 285.0 eV and at 187.5 eV respectively.

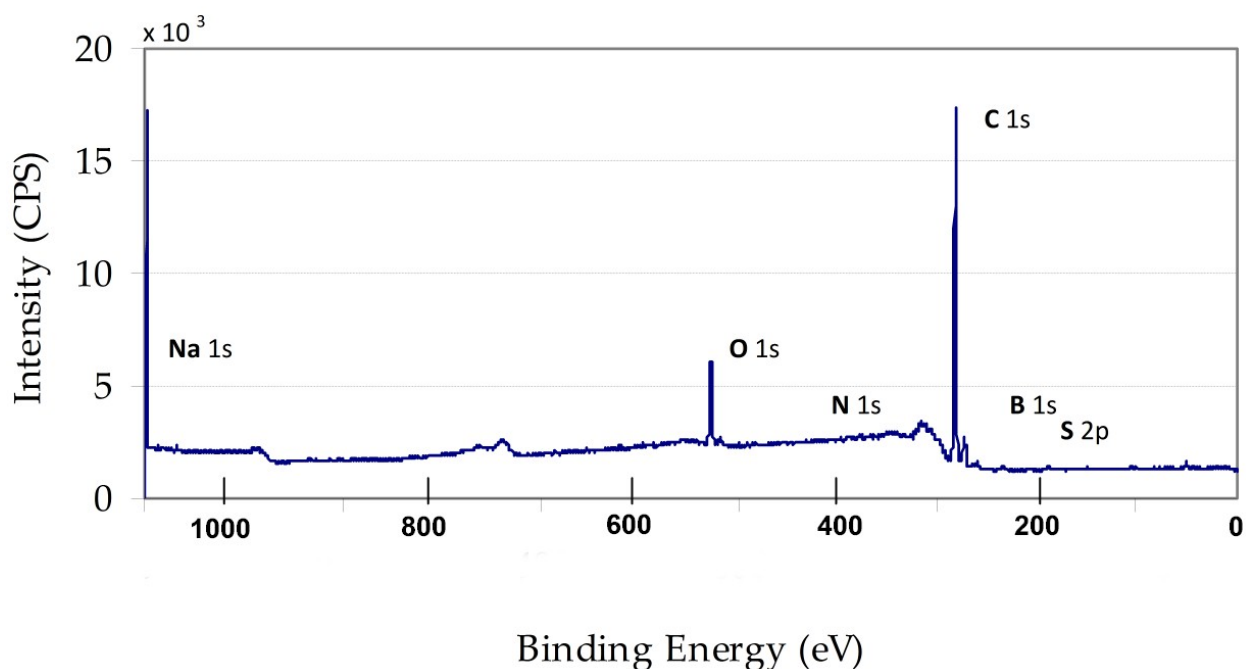


Figure 14: Survey scan of diamond powder (35-45 micron) treated with boron for 8 hours.

The data in Figure 14 indicates that the boron oxide peak is located at 194.0 eV. Since the pure boron peak is located at 190 eV, it is possible that the shift may be due to the boron compound found on the surface of the diamond. Chemical shifts are considered when they exceed 0.5 eV.

A similar result was observed for diamond powder in the size range of 5.5-8 microns. This XPS analysis is given in Figure 15.

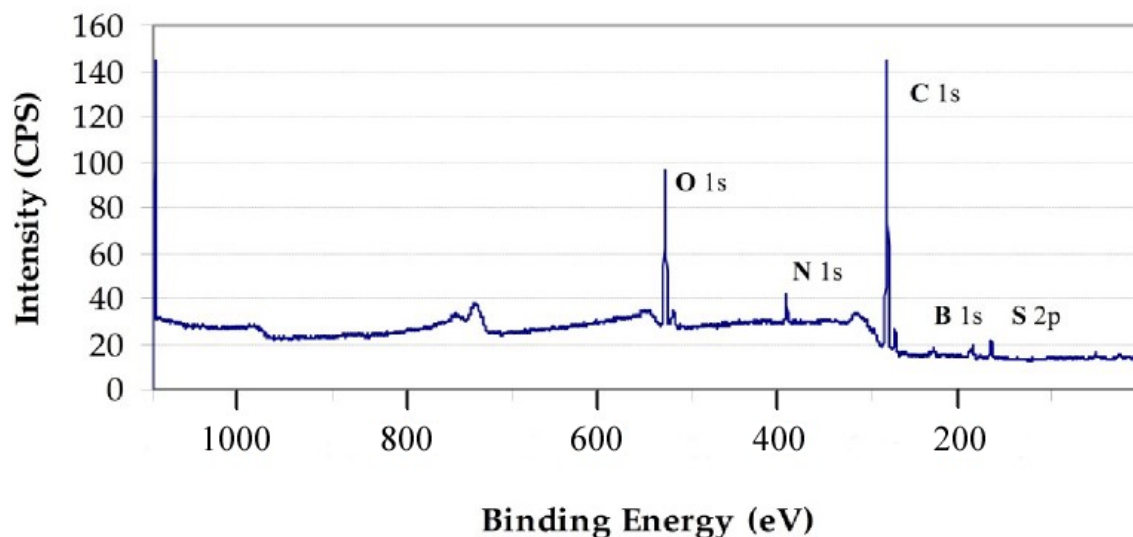


Figure 15: Survey scan of diamond powder (5.5-8 micron) treated with boron for 8 h.

It may be noted that the boron content of the sample was found to be 3910 ppm, which is discussed further, later in this report.

According to the XPS analysis, the boron peak was located at 189.5 eV with a FWHM of 4.236 eV. Table 5 provides data for the other elements found on the surface of the sample. Diamond powders 5.5-8 microns in size had more boron on the surface, and the treatment time was 8 h at 1200 °C.

Table 5: XPS analysis of 5.5-8 μm size diamond powder doped with boron.

Peak	Position BE (eV)	FWHM (eV)	Raw Area (CPS)	Atomic Mass	Atomic Conc. (%)	Mass Conc. (%)
O 1s	531.50	2.640	30135.9	15.999	19.44	23.67
N 1s	397.00	1.701	4484.1	14.007	3.23	3.44
C 1s	285.00	1.809	55847.4	12.011	65.25	59.63
B 1s	189.50	4.236	4537.6	10.823	10.03	8.26
S 2p	169.00	2.258	3854.8	32.065	2.05	5.01

Figure 16 shows a comparison between 5.5-8 micron size boron doped diamond powder and the untreated samples. The Boron peak is located at 189.5 eV with a FWHM of 4.236 for the control sample. The shift in the boron peak is evident in this figure. Also, the boron peak is closer to the XPS data for boron 1s.

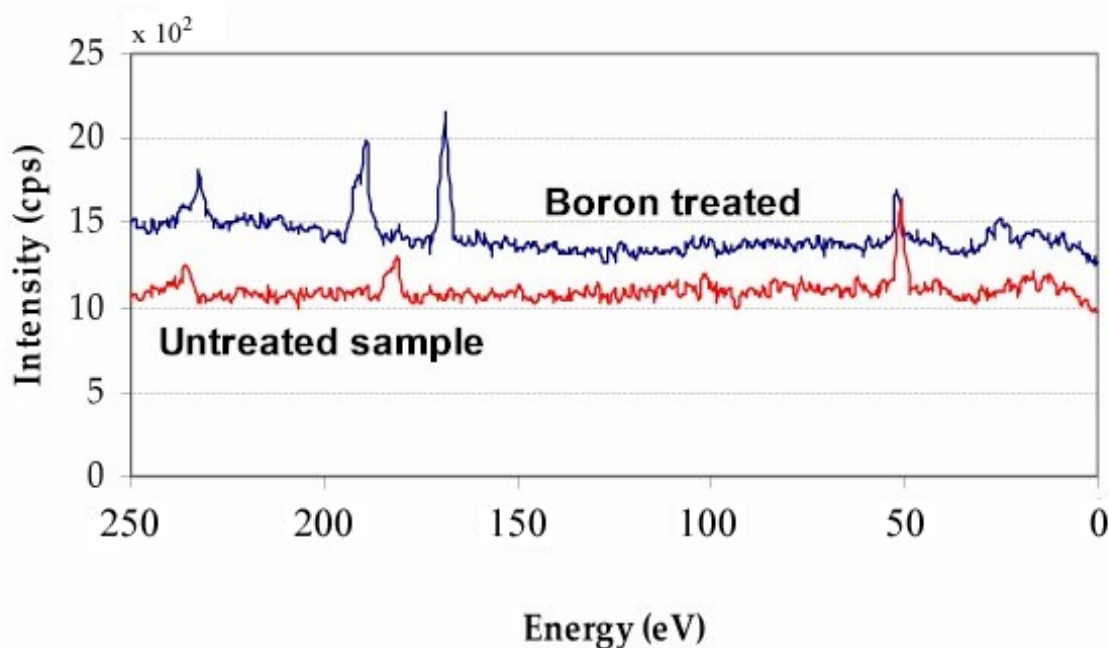


Figure 16: XPS survey scan comparison of boron treated diamond powder (5.5-8 microns) and the untreated sample.

As mentioned earlier, diamond powders of size range 5.5-8 microns had a higher boron concentration, 30,935 ppm, as obtained from PGNA. The sample was cleaned with the three step cleaning process, as mentioned earlier. Table 6 shows the XPS data for this sample.

Table 6: XPS data for boron treated 5.5-8 micron diamond powder.

Peak	Position BE (eV)	FWHM (eV)	Raw Area (CPS)	Atomic Mass	Atomic Conc. (%)	Mass Conc. (%)
O 1s	531.00	2.649	26758.9	15.999	14.21	17.50
N 1s	397.00	2.121	11860.5	14.007	9.12	9.83
C 1s	284.00	1.749	39237.6	12.011	49.00	45.31
B 1s	189.00	3.744	10248.3	10.823	24.21	20.17
Al 2p	73.50	2.975	2095.5	26.928	3.46	7.19

XPS survey scans of 5.5-8 micron diamond powder treated with boron is shown in Figure 17 and a comparison with untreated powder is given in Figure 18.

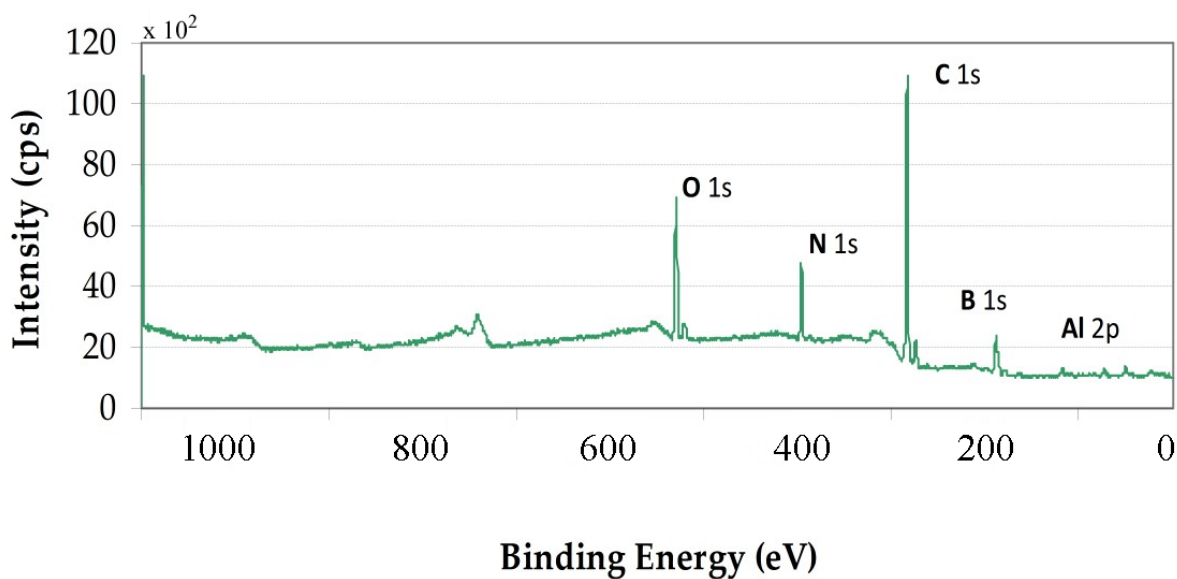


Figure 17: Survey scan of diamond powder (5.5-8 microns) treated with boron for 8 h.

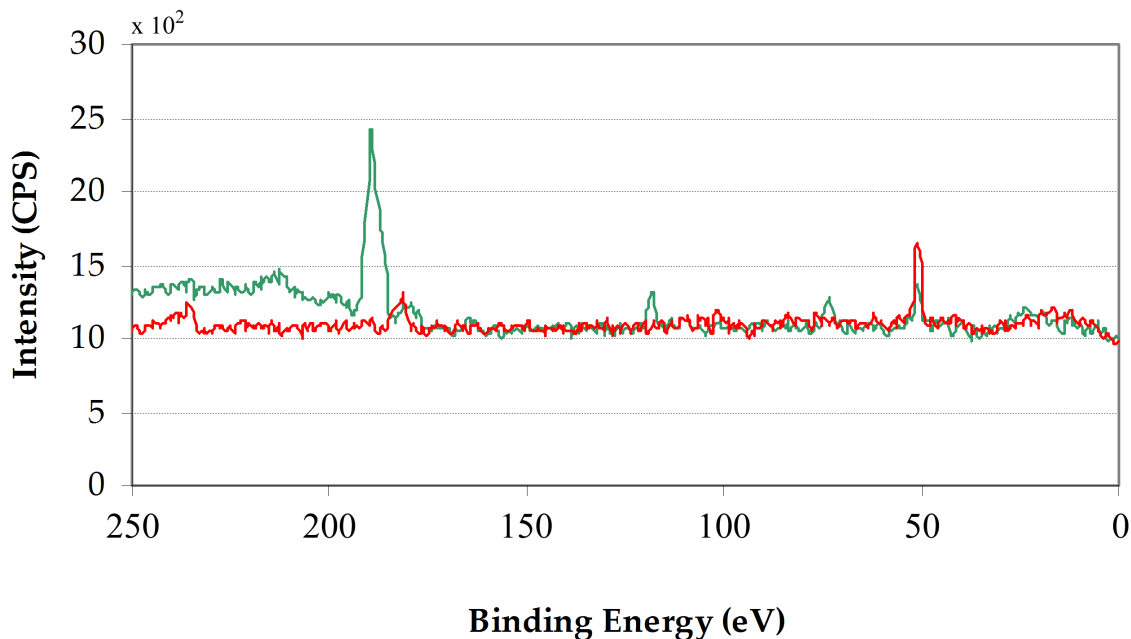


Figure 18: XPS survey scan comparison of diamond powder (5.5-8 microns) and untreated sample.

The untreated sample used for comparison with the treated sample showed only oxygen and carbon peaks. No boron peak was identified in this control sample. It was also noted that the intensity of the diamond peak of the treated sample was lower than that of the control sample. The mass concentration percent calculated from the survey scans for the diamond in the treated sample was 45.31%, compared to the untreated sample which was about 88.59%, suggests the presence of boron and other compounds.

Table 7: Results of the Concentration of Boron on the Micron-sized Diamond Powder in the Heating Process.

Sample	Description of Treatment	Concentration of Boron (%wt)
Control	Natural Diamond Powder (60-80 microns)	88% of diamond
#1	Ratio B/D = 5:1, Heated 1 hr. in each temperature increment step of 200, 400, and 600 °C in a hydrogen	0.267

Sample	Description of Treatment	Concentration of Boron (%wt)
	atmosphere. Cleaned once with HNO ₃ for 2 h.	
#2	Ratio B/D = 5:1, Heated 1 hr. in each temperature increment step of 200, 400, and 600 °C in an argon atmosphere. Cleaned once with HNO ₃ for 2 h.	2.100
#3	Ratio B/D = 3:1, Heated 1 hr. in each temperature increment step of 200, 400, and 600 °C in a hydrogen atmosphere. Cleaned once with HNO ₃ for 2 h.	1.010
#4	Ratio B/D = 3:1, Heated 2 hr. in each temperature increment step of 200, 400, and 600 °C in a hydrogen atmosphere. Cleaned once with HNO ₃ for 2 h.	1.270
#5	Ratio B/D = 3:1, Heated 4 hr. in each temperature increment step of 200, 400, and 600 °C in a hydrogen atmosphere. Cleaned once with HNO ₃ for 2 h.	0.097

B/D: Boron/Diamond ratio

It appears that the inert gas used during boron doping had some effect on the doping process. Under an argon atmosphere more boron could be diffused onto diamond. The boron concentration of other samples under various experimental conditions is given in Tables 7 and 8. The samples were treated for 1,2,4, or 8 hours at different temperatures.

Table 8: Results of Concentration of Boron on more Samples of Micron-sized Diamond Powder in the Heating Process.

Sample	Description of treatment	Concentration of Boron (ppm)
#6	Ratio B/D = 3:1, Heated 8 hrs. at 800 °C in Argon. Cleaned in three steps cleaning process.	54
#7	Ratio B/D = 2:1, Heated 8 hrs. at 800 °C in Argon. Cleaned in three steps cleaning process.	54
#8	Ratio B/D = 1:1, Heated 8 hrs. at 800 °C in Argon.	10

Sample	Description of treatment	Concentration of Boron (ppm)
	Cleaned in three steps cleaning process.	
#9	Ratio B/D = 5:1, Heated 1 hr. in each temperature increment step of 200, 400, and 600 °C in hydrogen. Cleaned in three steps cleaning process.	110
#10	Ratio B/D = 5:1, Heated 1 hr. in each temperature increment step of 200°C, 400°C, and 600°C in argon. Cleaned in three steps cleaning process.	24
#11	Ratio B/D = 3:1, Heated 1 hr. in each temperature increment step of 200, 400, and 600 °C in hydrogen. Cleaned in three steps cleaning process.	19
#12	Ratio B/D = 3:1, Heated 2 hr. in each temperature increment step of 200, 400, and 600°C in hydrogen. Cleaned in three steps cleaning process.	32
#13	Ratio B/D = 3:1, Heated 4 hr. in each temperature increment step of 200, 400, and 600°C in hydrogen. Cleaned in three steps cleaning process.	30
#14	Ratio B/D = 3:1, Heated 6 hr. in each temperature increment step of 200, 400, and 600°C in argon. Cleaned in three steps cleaning process.	20
#15	Ratio B/D = 3:1, Heated 2 hrs. in each temperature increment at 600, 900, 1030°C in hydrogen. Cleaned in three steps cleaning process.	1280

4.2 Irradiation Process at the University of Missouri Research Reactor (MURR)

Diamond powder samples were sent to MURR for irradiation in a neutron flux. Three to four grams of the boron doped samples were irradiated. The boron concentration in the samples was in the range of 3910 to 16200 ppm, as determined by PGNA. These samples were sealed in quartz tubes and irradiated for one minute at a nominal flux of 5×10^{13} to 8×10^{13} n / (cm³ s). These samples were irradiated in “Flooded Can Experiments Made.”

Some samples were irradiated again in the reactor pool. This time, the samples were sealed in quartz vials under “house” vacuum—around 1 to 2 mm of pressure to avoid oxygen

inside the vials. Then the samples were irradiated in the reactor pool for 24 hrs at a nominal flux of $8 \times 10^{13} \text{ n / (cm}^3 \text{ s)}$.

5.0 Adsorption Measurements

5.1 Krypton

A cold wall reactor was used initially under static condition to adsorb krypton onto diamond powder samples. The reactor is shown in Figure 26. The sample inside the reactor was heated electrically to the desired temperature. However, to prevent any damage to the reactor wall while an experiment is running, cold water was flowed through the wall of the reactor. The water flow keeps the wall of the reactor cold while the inside of the reactor reaches high temperatures.



Figure 19: External view of the cold wall reactor system.

The internal setup of the reactor can be seen in Figure 20. Various important components of the system are labeled. The power source is connected to the system through electrical connectors labeled *A*. The component *B* is the filament wire. The wire is made up of tungsten and can withstand the high temperatures used in this project. The wire is wrapped around a boron nitride cylinder labeled *C*. The cylinder was heated directly by the tungsten wire, which then transferred the heat to the sample. Boron nitride was used to reduce contamination into the

sample. Within the cylinder was another smaller cylinder of graphite labeled *D*, which is able to withstand the high temperatures. At the top of the graphite was the sample. The wire labeled *E* is the thermocouple. It is an Omega Type K thermocouple which allows accurate measurement in the temperature range used. The stand labeled *F* is made up of graphite.

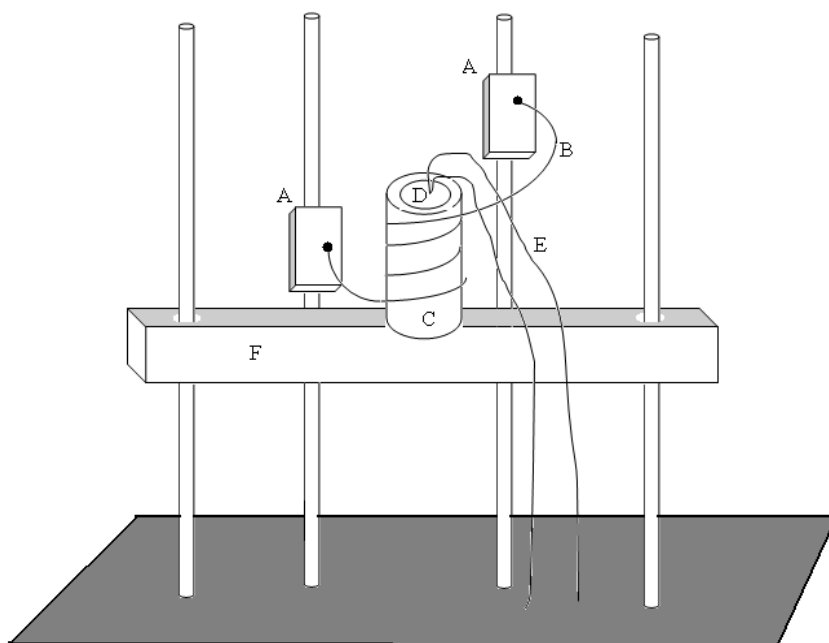


Figure 20: Internal view of the cold wall reactor system.

Once the sample was in place a vacuum pump was used to remove air from the reactor. This created a negative pressure within the system and helped to seal the lid to the base. When a higher temperature was needed helium was introduced into the system. By maintaining a constant vacuum with the vacuum pump while flowing helium into the reactor, a constant flow of helium at low vacuum was maintained in the reactor. The current to the system was increased slowly to raise the temperature of the sample. Once the temperature reached around 300 °C, the helium tank was shut off to flush the reactor of the off-gas that may have been present in the sample. This was performed twice to remove any air trapped inside the reactor. After the system was cleared of contaminants, the krypton gas was introduced in the reactor and was flushed with krypton two times. The vacuum pump was shut off to create a positive pressure of 15-30 psi. The power to the reactor was increased slowly until the desired temperature was reached. Table 9 lists the conditions under which the krypton adsorption experiments were conducted.

Table 9: Conditions of the 1st and 2nd trials.

	Experimental # 1	Experimental # 2
Sample	Poly Film	Poly Film Natural Crystal
Temperature	525°C	650°C
Pressure	45 psi	45-15 psi
Time	8 hrs	22 hrs

Following adsorption runs the samples were analyzed by NAA. Less than 30 ppb of krypton was reported in these two samples. Diamond powder samples were exposed to krypton in a similar manner. The NAA showed less than 100 ppb krypton content in the diamond sample. It was concluded that a temperature higher than 1000 °C may be necessary to increase the adsorption capacity of diamond for krypton. The cold wall reactor could not be operated at that temperature. Therefore a dynamic system described below in Figure 21 was designed and used.

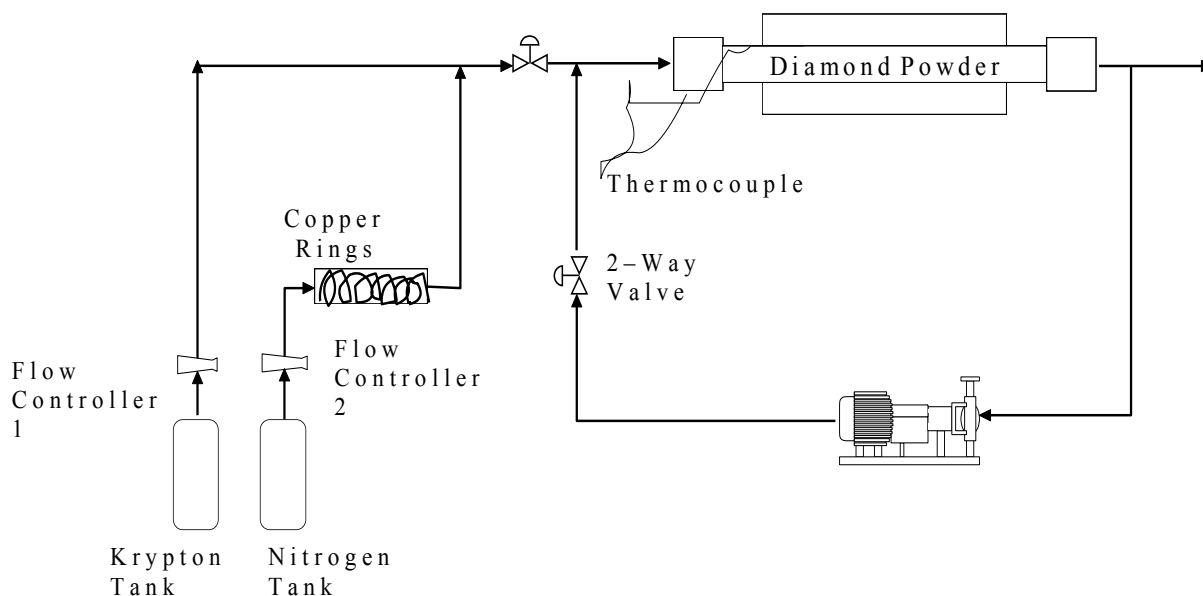


Figure 21: Dynamic apparatus used in krypton adsorption studies.

The system used in this experiment is shown in Figure 21. A mass flow controller was used to maintain krypton concentration and flow rate. Diamond powder was placed inside the ceramic tube and held approximately at the centre with the help of ceramic wool. Krypton gas was allowed to flow through a column of copper turnings. The column was wrapped with a flexible heating tape and the temperature was controlled by using a variable transformer and was set at 250°C. This arrangement removed any oxygen present in the gas stream by reacting it with copper. The gas from the other end of the ceramic tube was vented out. The furnace temperature was maintained at above 1300°C during the duration of the experiment. The Kr concentration was maintained at 2000 ppm and the flow rate was maintained at 20 ml/min.

Two runs were conducted with the dynamic experimental system. The samples were then analyzed for krypton concentration by NAA. Table 10 lists the specifications of the experiment and the krypton concentration reported by NAA analysis.

Table 10: Kr adsorption for the following diamond samples at high temperatures.

Sample	Diamond Powder Size	Weight	Furnace Temperature	Kr Flow Rate	Time	Concentration measured by NAA
	(μm)	(g)	($^{\circ}\text{C}$)	(ml/min)	(hrs)	(ppm)
A	60-80	1	1300	9	8	114
B	5.5-8	2	1066	25	8	110.4
C	0-0.25	2	1140	25	8	155.3
D	270/325 mesh	2	1116	25	8	26.4

5.2 Iodine

Iodine adsorption on diamond powder was studied at four different temperatures. Table 11 gives the conditions of the experiments.

Table 11: Experimental Conditions for Iodine Adsorption.

Sample	Diamond Powder Size	Weight	Iodine Vapour Concentration	Temperatures
	(μm)	(g)	(ppm)	($^{\circ}\text{C}$)
E	5.5-8	1	7.2	203
F	5.5-8	1	7.2	401
G	5.5-8	1	7.2	601
H	60-80	1	7.2	498

Breakthrough curves for Iodine concentration at different temperatures were plotted and are shown in the figures below. Again the adsorption is very low. We also explored fluorescence techniques for Iodine detection in the flow stream to quantify the adsorption better, but we could not resolve sensitivity issues within the time frame of the project.

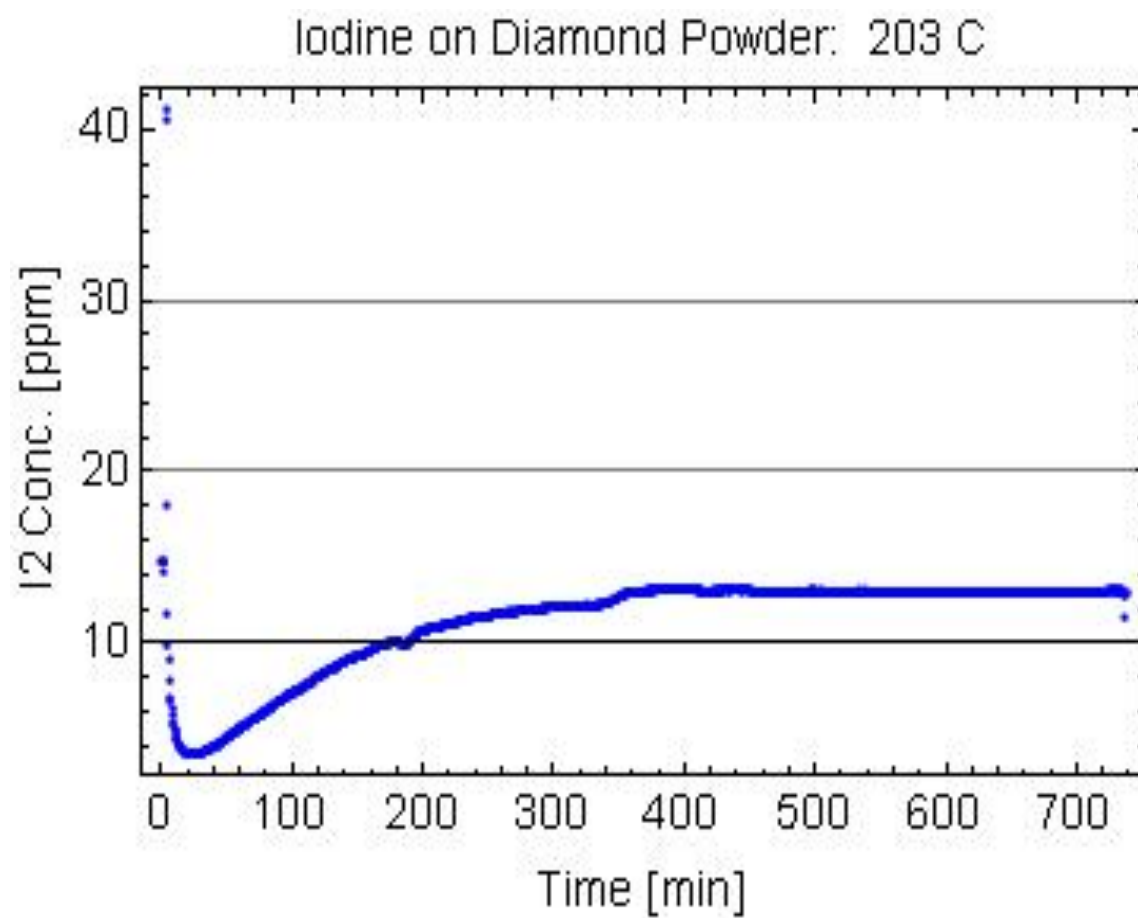


Figure 22: Breakthrough curve for I₂ concentration for Sample E at 203 °C.

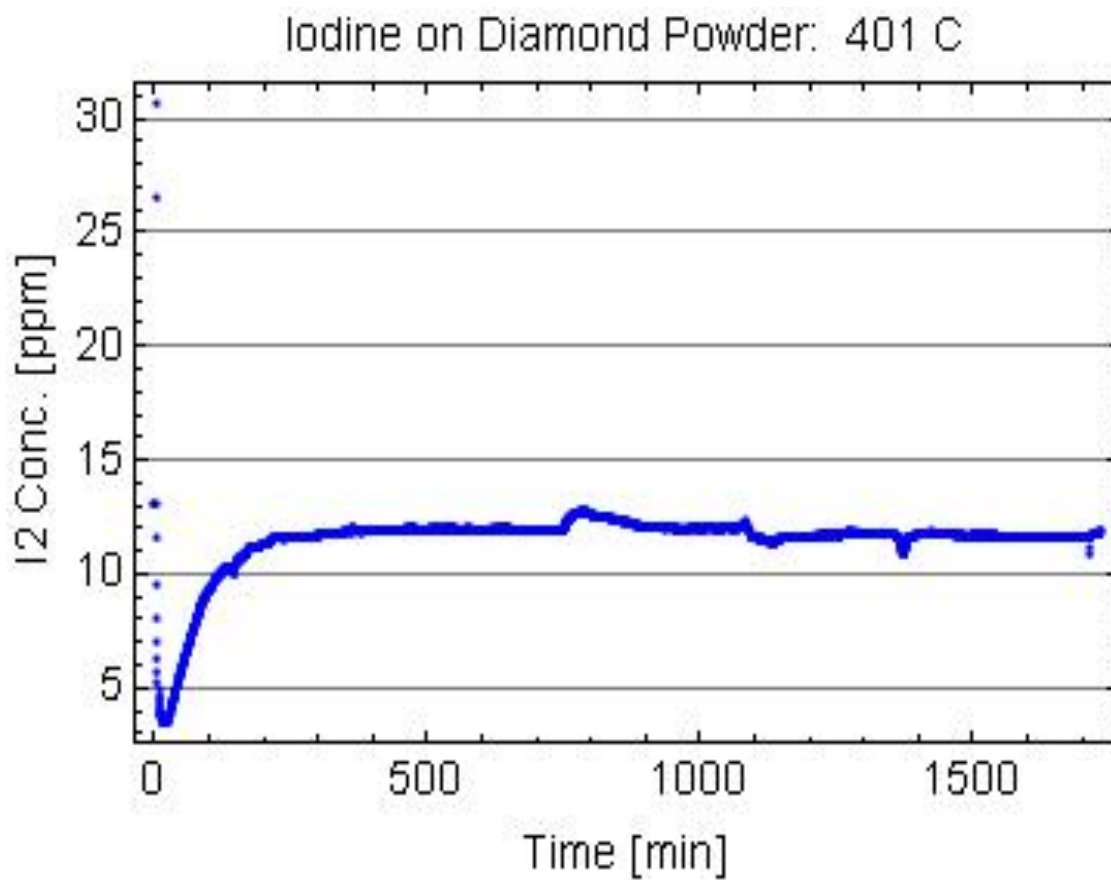


Figure 23: Breakthrough cure for I₂ concentration for Sample F at 401 °C.

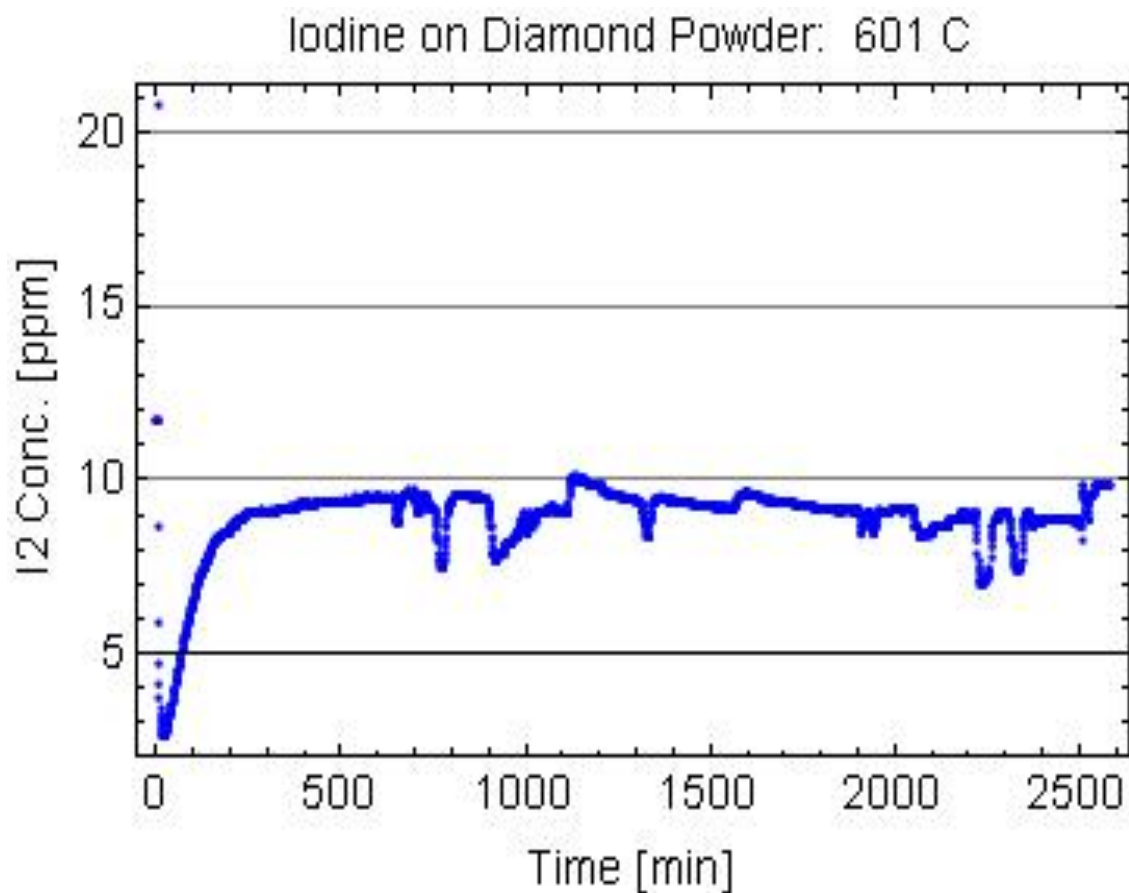


Figure 24: Breakthrough cure for I₂ concentration for Sample G at 601°C

5.3 Krypton and Iodine co-adsorption

We carried out additional measurements on Iodine and Krypton co-adsorption, and the data are shown in Table 12 below. Again we did not observe any significant adsorption.

Table 12: Simultaneous Krypton and Iodine Adsorption

Sample	Diamond Powder Size	Weight	Furnace Temp	Kr Flow Rate	Time	Kr Conc. measured by NAA	I ₂ Conc. measured by NAA
	(μm)	(g)	(°C)	(ml/min)	(hrs)	(ppm)	(ppm)
I	0-0.25	2	968	130.8		<1	1.4
J	270/325 mesh	2	1004	130.8	8	<0.1	1.9

6.0 Carbon dioxide Adsorption

6.1 Experimental Section

6.1.1 Materials

The silica gel used in this study was Grade 40, 6 x 12 mesh (Lot # MIL-D-3716 Type II). Molecular sieve-13X was Grade 544. Both silica gel and molecular sieves were supplied by Davison Chemical Company. Activated carbon, Type BPL, was obtained from Calgon Carbon Corporation. The properties of these adsorbents are presented in Table 13. Carbon dioxide was purchased from Midwest Airgas, Inc., Columbia, Missouri, and had a stated purity of 99.5%.

6.1.2 Static Adsorption Apparatus

Adsorption and desorption studies were carried out gravimetrically in two all glass apparatus using two electrobalances, a Cahn C-2000 and a Cahn D-100. The D-100 electrobalance has a capacity of up to 100 grams with a sensitivity of 10 μg . The sample weight was recorded in a computer, interfaced to the electrobalance control unit. The software package provided with the electrobalance is capable of displaying the sample weight on the screen, as well as transferring the results to a printer. The C-2000 is capable of measuring up to 3.5 g with a sensitivity of 1 μg . The sample weight was monitored with a strip chart recorder connected to the control unit of the electrobalance.

During studies with binary mixtures, two sample loops were utilized to collect the samples before and after equilibrium was attained. One sample loop was connected to the mixing chamber and the other to the adsorption chamber. Two remote electrical switching valves (6-port) were used with helium as a carrier gas to sweep the samples in the gas chromatograph. One pore of the valve was connected directly to a vacuum pump. The helium remaining in the sample loop was evacuated by a pump before switching the loop to the respective chambers.

A water bath and a copper circulation coil wrapped around the sample hangdown tube were used to control the temperature to within $\pm 0.1^\circ\text{C}$ of the desired value during adsorption and desorption experiments. A heating tape was used to obtain temperatures up to 227°C when regenerating the samples. The temperature was controlled by a Staco Energy Products Co. voltage regulator (variac). The vacuum system consisted of two mechanical roughing pumps, a sorption trap cooled with a dry ice bath, and a Type VMF diffusion pump manufactured by CVC

products, Inc. A vacuum of 10^{-4} mmHg could be obtained in the system prior to initiating an adsorption run. Pressure up to 10^{-3} mmHg were measured by two convection gauges. The convection gauges were monitored by a vacuum gauge controller, Model 307, manufactured by Granville-Phillips Company. The leak rate of the complete system was approximately 0.001 mmHg/hr. Equilibrium pressures were measured with a Wallace and Tiernan absolute pressure gauge whose calibration is traceable to the National Institute of Standards and Technology. The helium remaining in the sample loop was evacuated by a pump before switching the loop to the respective chambers.

Table 13: Properties of Solid Adsorbents.

Property (unit)	BPL Activated Carbon	Silica Gel (Grade 40)	Molecular Sieve 13X
Particle size, (Å) ^b	6 x 16 mesh	6 x 12 mesh	8 x 12 mesh
Surface area, (m ² /g) ^a			
micropores	823	663	294
meso and macropores	50	9	101
total	873	672	395
Average pore diameter 4V/S (Å) ^a	26	24	41.7 ^c
Bulk density (g cm ⁻³) ^b	0.60	0.72	0.72
Equilibrium water capacity (% wt.) ^b	-	-	29.5
Moister content as shipped (% wt.) ^b	< 1	-	< 1.5

^a Analysis made by Porous Materials, Inc. Ithaca, New York.

^b Analysis provided by the manufacturer.

^c Based on total surface area and pore volume.

Table 14: Equilibrium Adsorption Data for Carbon Dioxide on Molecular Sieve-13X.

15°C		25°C		35°C	
Pressure	Uptake	Pressure	Uptake	Pressure	Uptake
mmHg	g/g	mmHg	g/g	mmHg	g/g
(MS-CO2-308-1)					
14.1	0.063	5.0	0.027	11.0	0.014
38.5	0.092	9.8	0.043	20.4	0.035
50.0	0.104	25.6	0.068	35.9	0.052
60.6	0.112	39.9	0.081	50.1	0.064
70.1	0.117	60.3	0.097	60.9	0.070
82.5	0.121	81.5	0.108	75.4	0.079
100.5	0.126	98.9	0.115	102.5	0.092
135.0	0.135	122.5	0.124	132.0	0.102
160.1	0.139	159.9	0.132	160.0	0.111
200.5	0.144	211.5	0.139	207.5	0.123
		Run #2		Run #3	
		7.9	0.030	8.9	0.013
		20.3	0.056	20.4	0.034
		33.9	0.074	35.0	0.050
		50.8	0.088	45.4	0.059
		61.1	0.096	59.7	0.069
		80.1	0.106	80.0	0.080
		102.0	0.114	107.0	0.093
		129.5	0.120	128.9	0.101
		160.0	0.126	157.8	0.109

15°C		25°C		35°C	
Pressure	Uptake	Pressure	Uptake	Pressure	Uptake
mmHg	g/g	mmHg	g/g	mmHg	g/g
(MS-CO2-308-1)					
		201.0	0.133	199.8	0.121

Table 15: Equilibrium Adsorption Data for Carbon Dioxide on Activated Carbon at 25°C.

Run #1		Run #2	
Pressure	Uptake	Pressure	Uptake
mmHg	mg/g	mmHg	mg/g
4.1	1.587	5.9	1.993
12.2	3.931	11.1	3.584
20.8	6.183	21.2	6.187
31.5	8.727	31.0	8.362
40.0	10.576	41.1	10.593
52.5	13.140	59.1	14.217
70.9	16.581	78.5	16.742
101.0	21.762	99.0	21.185
130.0	26.302	130.0	26.221
160.0	30.484	161.0	30.860
204.1	36.288	198.9	35.849

Table 16: Equilibrium Adsorption Data for Carbon Dioxide on Silica Gel at 25°C.

Run #1		Run #2	
Pressure	Uptake	Pressure	Uptake
mmHg	mg/g	mmHg	mg/g
11.3	1.175	7.2	1.147
21.2	2.785	23.0	2.965
35.8	4.156	30.0	3.700
47.0	5.175	70.0	7.471
58.9	6.224	80.0	8.367
80.1	7.995	92.5	9.486
99.1	9.514	105.0	10.507

7.0 Process Optimization

We had wanted to explore simulation of the boron diffusion processes in diamond, molecular dynamics calculations for adsorption, and design parameters for a diamond powder bed, as guided by the experimental data. While we realized some progress in modeling of the bed, since the data did not show any significant adsorption of Krypton and Iodine on all diamonds we studied, we remained focused on getting more data and improving the quality of the data.

We describe below our progress towards modeling of the bed. However we assume certain operating conditions and adsorbant geometry, and equilibrium adsorption data. As the flow of the fluid continues, the bed becomes saturated, and a concentration distribution is established within the bed.

At time t_i the adsorbate first appears in the effluent stream. The time t_b is defined as the time required to reach the breakpoint concentration, which is indicated by C_b . The time from t_i to t_b corresponds to the thickness of the adsorption or mass transfer zone in the bed.

7.1 Material Balance in a Packed Bed Adsorbed

The adsorption in a packed bed can be modeled using the shell balance method. This mass balance equation is Eq 1:

$$\begin{aligned} \varepsilon S \left[-D_{Ad} \frac{\partial C_A}{\partial Z} + C_A U_Z \right]_{Z,t} - \varepsilon S \left[-D_{Ad} \frac{\partial C_A}{\partial Z} + C_A U_Z \right]_{Z+\Delta Z,t} = \\ \left[S \Delta Z \varepsilon \frac{\partial C_A}{\partial t} + C_A U_Z \right]_Z + \left[S \Delta Z (1 - \varepsilon) \frac{\partial C_{As}}{\partial t} \right]_Z \end{aligned} \quad (1)$$

Where

ε = void fraction in the bed,

S = cross-sectional area of the column,

D_{Ad} = effective axial diffusion coefficient of A,

C_A = concentration of A in the fluid phase, mol/cm³,

C_{As} = average concentration of A in the solid phase, mol/cm³,

U_z = interstitial velocity.

Neglecting diffusion, and dividing by $(1 - \varepsilon)S\Delta Z$,

$$-\frac{\varepsilon U_z}{1-\varepsilon} \left[\frac{\partial C_A}{\partial Z} \right]_t - \frac{\varepsilon}{1-\varepsilon} \left[\frac{\partial C_A}{\partial t} \right]_Z = \left[\frac{\partial C_{As}}{\partial t} \right]_z \quad (2)$$

The velocity was assumed to be constant. It is further assumed that the mass transfer to the solid adsorbent is controlled by the fluid-phase mass transfer coefficient, and the equilibrium between the fluid and solid phases can be described by a linear isotherm equation.

Introducing $\rho_s = \rho_b / (1 - \varepsilon)$ and $q_A = C_{As} / \rho_s$ into Eq. (2), the following expression is obtained. Eq 8.3:

$$\left[\frac{\partial C_A}{\partial t} \right]_Z = -U_z \left[\frac{\partial C_A}{\partial Z} \right]_Z - \frac{p_b}{\varepsilon} \left[\frac{\partial q_A}{\partial t} \right]_z \quad (3)$$

The change in adsorbate content of the adsorbent and of the fluid may be expressed in terms of the rate of adsorption Eq 4:

$$\left[\frac{\partial q_A}{\partial t} \right]_z = \frac{K_f a}{p_b} (C_A - C_A^*) \quad (4)$$

Where C_A^* is the concentration of adsorbate A in the fluid phase that is in equilibrium with the solid. For a linear isotherm, the equilibrium fluid-phase concentration is related to the concentration in the solid by the expression Eq 5.

$$q_A = K_D C_A^*, \text{ or, } q_A^\infty = K_D C_{A0} \quad (5)$$

Where K_D is the distribution coefficient and q_A^∞ is the saturation capacity of the bed and when the concentration of the solute in the influent is C_{A0} . Therefore, Equation (4) can be rewritten as Eq 6.

$$\left[\frac{\partial q_A}{\partial t} \right]_z = \frac{K_f a}{p_b} \left(C_A - \frac{1}{K_D} q_A \right) \quad (6)$$

Equation (6) and the mass balance equation can be simplified by rewriting them in terms of the following dimensionless variables:

$$\zeta = \frac{Z K_f a}{\varepsilon U_z}, \quad (7)$$

$$\tau = \frac{K_f a}{K_D p_b} \left(t - \frac{Z}{U_z} \right), \quad (8)$$

$$X^* = \frac{C_A}{C_{A0}}, \quad (9)$$

and

$$Q^* = \frac{q_A}{q_A^\infty} = \frac{q_A}{K_D C_{A0}}. \quad (10)$$

We can express equations (3) and (6) in terms of the dimensionless variables as.

$$\frac{\varepsilon}{p_b K_D} \left[\frac{\partial X^*}{\partial \tau} \right] = - \left[\frac{\partial X^*}{\partial \zeta} \right] - X^* + Q^* \quad (11)$$

and

$$\left[\frac{\partial Q^*}{\partial \tau} \right] = X^* - Q^* \quad (12)$$

For the case in which the adsorbate concentration is constant at the bed inlet and the initial solute concentration in the bed is zero, the boundary and initial conditions are Eq 13:

$$C_A = C_{A0}, \text{ at } Z = 0, X^* = 1, \zeta = 1, \quad (13)$$

and

$$q_A = 0, t - \frac{Z}{U_z} = 0, Q^* = 0, \tau = 0. \quad (14)$$

We programmed these equations and we were able to obtain results for the concentrations in the gas and the solid phase as functions of various parameters. For the case of carbon dioxide, and silica gel, the best agreement between the experimental data and predicted values was observed for the carbon dioxide breakthrough from a mixed adsorbent bed with some assumptions regarding the mass transfer coefficient.

8.0 Students Supported

Name	Citizenship	Major
Surabhi Grover	India	Nuclear Engineering
Sangita Sharma	USA	Mechanical Engineering
Chris Amhez	USA	Nuclear Engineering
Joshua Schockle	USA	Nuclear Engineering
Yefer Surez	USA	Nuclear Engineering